Learning Dynamical Systems from Noisy Data with Inverse-Explicit Integrators

Anonymous Author(s)
Affiliation
Address
email

Abstract

We introduce the mean inverse integrator (MII), a novel approach to increase the accuracy when training neural networks to approximate vector fields of dynamical systems from noisy data. This method can be used to average multiple trajectories obtained by numerical integrators such as Runge–Kutta methods. We show that the class of mono-implicit Runge–Kutta methods (MIRK) has particular advantages when used in connection with MII. When training vector field approximations, explicit expressions for the loss functions are obtained when inserting the training data in the MIRK formulae, unlocking symmetric and high order integrators that would otherwise be implicit for initial value problems. The combined approach of applying MIRK within MII yields a significantly lower error compared to the plain use of the numerical integrator without averaging the trajectories. This is demonstrated with experiments using data from several (chaotic) Hamiltonian systems. Additionally, we perform a sensitivity analysis of the loss functions under normally distributed perturbations, supporting the favourable performance of MII.

1 Introduction

Recently, many deep learning methodologies have been introduced to increase the efficiency and quality of scientific computations [1, 2, 3, 4]. In physics-informed machine learning, deep neural networks are purposely built so to enforce physical laws. As an example, Hamiltonian neural networks (HNNs) [5] aim at learning the Hamiltonian function from temporal observations. The Hamiltonian formalism was derived within classical mechanics for modelling a wide variety of physical systems. The temporal evolution of such systems is fully determined when the Hamiltonian function is known, and it is characterized by geometric properties such as the preservation of energy, the symplectic structure and the time-reversal symmetry of the flow [6, 7].

Numerical integrators that compute solutions preserving such properties are studied in the field of geometric numerical integration [7, 8]. Thus, deep learning, classical mechanics and geometric numerical integration are all relevant to the development of HNNs. In this work, we try to identify the optimal strategy for using numerical integrators when constructing loss functions for HNNs that are trained on noisy and sparse data.

Generally, we aim at learning autonomous systems of first-order ordinary differential equations (ODE)

$$\frac{d}{dt}y = f(y(t)), \quad y : [0, T] \to \mathbb{R}^n. \tag{1}$$

In the traditional setting, solving an initial value problem (IVP) means computing approximated solutions $y_n \approx y(t_n)$ when the vector field $f(y)$ and an initial value $y(t_0) = y_0$ are known. The focus of our study is the corresponding inverse problem; assuming knowledge of multiple noisy samples of the solution, $S_N = \{\tilde{y}_n\}_{n=0}^N$, the aim is to approximate the vector field f with a neural

Submitted to 37th Conference on Neural Information Processing Systems (NeurIPS 2023). Do not distribute.

network model f_θ. We will assume that the observations originate from a (canonical) Hamiltonian system, with a Hamiltonian $H : \mathbb{R}^{2d} \to \mathbb{R}$, where the vector field is given by

$$f(y) = J\nabla H(y(t)), \quad J := \begin{bmatrix} 0 & I \\ -I & 0 \end{bmatrix} \in \mathbb{R}^{2d\times 2d}. \tag{2}$$

This allows for learning the Hamiltonian function directly by setting $f_\theta(y) = J\nabla H_\theta(y)$, as proposed initially in [5].

Recently, many works highlight the benefit of using symplectic integrators when learning Hamiltonian neural networks [9, 10, 11, 12]. Here, we study what happens if, instead of using symplectic methods, efficient and higher-order MIRK methods are applied for inverse problems. We develop different approaches and apply them to learn highly oscillatory and chaotic dynamical systems from noisy data. The methods are general, they are not limited to separable Hamiltonian systems, and could indeed be used to learn any first-order ODE. However we focus our study on Hamiltonian systems, in order to build on the latest research on HNNs. Specifically, we compare our methods to the use of symplectic integrators to train Hamiltonian neural networks. Our contributions can be summarized as follows:

- We introduce the **mean inverse integrator** (MII), which efficiently averages trajectories of MIRK methods in order to increase accuracy when learning vector fields from noisy data (Definition 5.1).
- We present an **analysis of the sensitivity** of the loss function to perturbations giving insight into when the MII method yields improvement over a standard one-step scheme (Theorem 5.2).
- We show that **symplectic MIRK** methods have at most order $p = 2$ (Theorem 4.4). Particularly, the second-order implicit midpoint method is the symplectic MIRK method with minimal number of stages.

Finally, numerical experiments on several Hamiltonian systems benchmark MII against one-step training and symplectic recurrent neural networks (SRNN) [10], which rely on the Störmer–Verlet integrator. The structural difference between these three approached is presented in Figure 2. Additionally, we demonstrate that substituting Störmer–Verlet with the classic Runge–Kutta method (RK4) in the SRNN framework yields significant reduction in error and allows accurate learning of non-separable Hamiltonian systems.

2 Related work

Hamiltonian neural networks was introduced in [5]. The numerical integration of Hamiltonian ODEs and the preservation of the symplectic structure of the ODE flow under numerical discretization have been widely studied over several decades [8, 7]. The symplecticity property is key and could inform the neural network architecture [13] or guide the choice of numerical integrator, yielding a theoretical guarantee that the learning target is actually a (modified) Hamiltonian vector field [14, 9], building on the backward error analysis framework [8]. Discrete gradients is an approach to numerical integration that guarantees exact preservation of the (learned) Hamiltonian, and an algorithm for training Hamiltonian neural networks using discrete gradient integrators is developed in [15] and extended to higher order in [16].

Since we for the inverse problem want to approximate the time-derivative of the solution, f, using only $\tilde{y}_n$, we need to use a numerical integrator when specifying the neural network loss function. For learning dynamical systems from data, explicit methods such as RK4 are much used [5, 17, 18]. However, explicit methods cannot in general preserve time-symmetry or symplecticity, and they often have worse stability properties compared to implicit methods [19]. Assuming that the underlying Hamiltonian is separable allows for explicit integration with the symplectic Störmer–Verlet method, which is exploited in [10, 20]. Symplecticity could be achieved without the limiting assumption of separability by training using the implicit midpoint method [12]. As pointed out in [12], this integrator could be turned into an explicit method in training by inserting sequential training data $\tilde{y}_n$ and $\tilde{y}_{n+1}$. In fact, the MIRK class [21, 22] contains all Runge–Kutta (RK) methods (including the midpoint method) that could be turned into explicit schemes when inserting the training data. This is exploited in [23], where high-order MIRK methods are used to train HNNs, achieving accurate

interpolation and extrapolation of a single trajectory with large step size, few samples and assuming zero noise.

The assumption of noise-free data limits the potential of learning from physical measurements or applications on data sets from industry. This issue is addressed in [10], presenting symplectic recurrent neural networks (SRNN). Here, Störmer–Verlet is used to integrate multiple steps and is combined with initial state optimization (ISO) before computing the loss. ISO is applied after training f_θ a given number of epochs and aims at finding the optimal initial value $\hat{y}_0$, such that the distance to the subsequent observed points $\tilde{y}_1, \dots, \tilde{y}_N$ is minimized when integrating over f_θ. While [10] is limited by only considering separable systems, [24] aims at identifying the optimal combination of third order polynomial basis functions to approximate a cubic non-separable Hamiltonian from noisy data, using a Bayesian framework.

3 Background on numerical integration

Some necessary and fundamental concepts on numerical integration and the geometry of Hamiltonian systems are presented below to inform the discussion on which integrators to use in inverse problems. Further details could be found in Appendix C.

Fundamental concepts: An important subclass of the general first-order ODEs (1) is the class of Hamiltonian systems, as given by (2). Often, the solution is partitioned into the coordinates $y(t) = [q(t), p(t)]^T$, with $q(t), p(t) \in \mathbb{R}^d$. A separable Hamiltonian system is one where the Hamiltonian could be written as the sum of two scalar functions, often representing the kinetic and potential energy, that depend only on q and p respectively, this means we have $H(q,p) = H_1(q) + H_2(p)$.

The h flow of an ODE is a map $\varphi_{h,f} : \mathbb{R}^n \to \mathbb{R}^n$ sending an initial value $y(t_0)$ to the solution of the ODE at time $t_0 + h$, given by $\varphi_{h,f}(y(t_0)) := y(t_0 + h)$. A numerical integration method $\Phi_{h,f} : \mathbb{R}^n \to \mathbb{R}^n$ is a map approximating the exact flow of the ODE, so that

$$y(t_1) \approx y_1 = \Phi_{h,f}(y_0).$$

Here, $y(t_n)$ represents the exact solution and we denote with y_n the approximation at time $t_n = t_0 + nh$. It should be noted that the flow map satisfies the following group property:

$$\varphi_{h_1,f} \circ \varphi_{h_2,f}\big(y(t_0)\big) = \varphi_{h_1,f}\big(y(t_0 + h_2)\big) = \varphi_{h_1+h_2,f}(y(t_0)). \tag{3}$$

In other words, a composition of two flows with step sizes h_1, h_2 is equivalent to the flow map over f with step size $h_1 + h_2$. This property is not shared by numerical integrators for general vector fields. The order of a numerical integrator $\Phi_{h,f}$ characterizes how the error after one step depends on the step size h and is given by the integer p such that the following holds:

$$\|y_1 - y(t_0 + h)\| = \|\Phi_{h,f}(y_0) - \varphi_{h,f}(y(t_0))\| = \mathcal{O}(h^{p+1}).$$

Mono-implicit Runge–Kutta methods: Given vectors $b, v \in \mathbb{R}^s$ and a strictly lower triangular matrix $D \in \mathbb{R}^{s\times s}$, a MIRK method is a Runge–Kutta method where $A = D + vb^T$ [25, 26] and we assume that $[A]_{ij} = a_{ij}$ is the stage-coefficient matrix. This implies that the MIRK method can be written on the form

$$\begin{aligned} y_{n+1} &= y_n + h\sum_{i=1}^{s} b_i k_i, \\ k_i &= f\big(y_n + v_i(y_{n+1} - y_n) + h\sum_{j=1}^{s} d_{ij}k_j\big). \end{aligned} \tag{4}$$

Specific MIRK methods and further details on Runge–Kutta schemes is discussed in Appendix C.2.

Symplectic methods: The flow map of a Hamiltonian system is symplectic, meaning that its Jacobian $\Upsilon_\varphi := \frac{\partial}{\partial y}\varphi_{h,f}(y)$ satisfies $\Upsilon_\varphi^T J \Upsilon_\varphi = J$, where J is the same matrix as in (2). As explained in [8, Ch. VI.2], this is equivalent to the preservation of a projected area in the phase space of $[q,p]^T$. Similarly, a numerical integrator is symplectic if its Jacobian $\Upsilon_\Phi := \frac{\partial}{\partial y_n}\Phi_{h,f}(y_n)$ satisfies $\Upsilon_\Phi^T J \Upsilon_\Phi = J$. It is possible to prove [8, Ch. VI.4] that a Runge–Kutta method is symplectic if and only if the coeffients satisfy

$$b_i a_{ij} + b_j a_{ji} - b_i b_j = 0, \quad i,j = 1,\dots,s. \tag{5}$$

4 Numerical integration schemes for solving inverse problems

We will now consider different ways to use numerical integrators when training Hamiltonian neural networks and present important properties of MIRK methods, a key component of the MII that is presented in Chapter 5.

Inverse ODE problems in Hamiltonian form: We assume to have potentially noisy samples $S_N = \{\tilde{y}\}_{n=0}^{N}$ of the solution of an ODE with vector field f. The inverse problem can be formulated as the following optimization problem:

$$\arg\min_{\theta} \sum_{n=0}^{N-1} \left\| \tilde{y}_{n+1} - \Phi_{h,f_\theta}(\tilde{y}_n) \right\|, \tag{6}$$

where $f_\theta = J\nabla H_\theta$ is a neural network approximation with parameters θ of a Hamiltonian vector field f, and Φ_{h,f_θ} is a one-step integration method with step length h. In the setting of inverse ODE problems, the availability of sequential points S_N could be exploited when a numerical method is used to form interpolation conditions, for $f_\theta \approx f$ for each n in the optimization problem (6). For example, $\tilde{y}_n$ and $\tilde{y}_{n+1}$ could be inserted in the implicit midpoint method, turning a method that is implicit for IVPs into an explicit method for inverse problems:

$$\Phi_{h,f_\theta}(\tilde{y}_n, \tilde{y}_{n+1}) = \tilde{y}_n + h f_\theta\Big(\frac{\tilde{y}_n + \tilde{y}_{n+1}}{2}\Big). \tag{7}$$

We denote this as the inverse injection, which defines an inverse explicit property for numerical integrators.

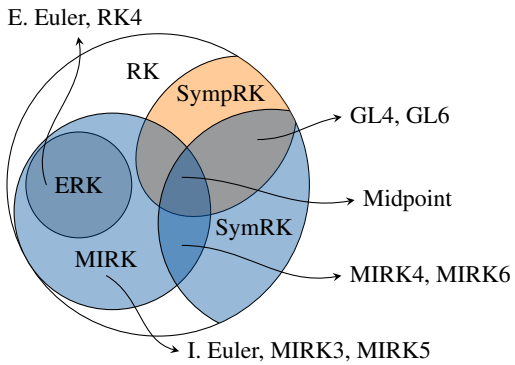

Figure 1: Venn diagram of Runge–Kutta (RK) subclasses: explicit RK (ERK), symplectic RK (SympRK), mono-implicit RK (MIRK) and symmetric RK (SymRK).

Definition 4.1 (Inverse injection)**.** Assume that $\tilde{y}_n, \tilde{y}_{n+1} \in S_N$. Let the *inverse injection* for the integrator $\Phi_{h,f}(y_n, y_{n+1})$ be given by the substitution $(\tilde{y}_n, \tilde{y}_{n+1}) \to (y_n, y_{n+1})$ such that

$$\hat{y}_{n+1} = \Phi_{h,f}(\tilde{y}_n, \tilde{y}_{n+1}).$$

Definition 4.2 (Inverse explicit)**.** A numerical one-step method Φ is called *inverse explicit* if it is explicit under the inverse injection.

This procedure is utilized successfully by several authors when learning dynamical systems from data, see e.g. [12, 27]. However, this work is the first attempt at systematically exploring numerical integrators under the inverse injection, by identifying the MIRK methods as the class consisting of inverse explicit Runge–Kutta methods.

Proposition 4.3. *MIRK-methods are inverse explicit.*

Proof. Since the matrix D in (4) is strictly lower triangular, the stages are given by

$$\begin{aligned} k_1 &= f(y_n + v_i(y_{n+1} - y_n)) \\ k_2 &= f(y_n + v_i(y_{n+1} - y_n) + h d_{21} k_1) \\ &\vdots \\ k_s &= f(y_n + v_i(y_{n+1} - y_n) + h \sum_{j=1}^{s-1} d_{sj} k_j) \end{aligned}$$

meaning that if y_n and y_{n+1} are known, all stages, and thus the next step $\hat{y}_{n+1} = y_n + h\sum_{i=1}^{s} b_i k_i$, could be computed explicitly. □

Because of their explicit nature when applied to inverse ODE problems, MIRK methods are an attractive alternative to explicit Runge–Kutta methods; in contrast to explicit RK methods, they can be symplectic or symmetric, or both, without requiring the solution of systems of nonlinear

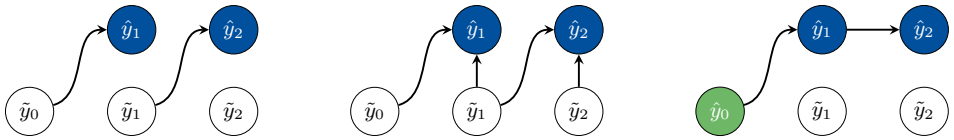

(a) ERK, one-step. (b) MIRK, one-step. (c) SRNN with ISO.

Figure 2: Differences of observation dependency, assuming $N = 2$ for explicit and mono-implicit one-step training, and explicit multi-step training with initial state optimization (green node $\hat{y}_0$).

equations, even when the Hamiltonian is non-separable. Figure 1 illustrates the relation between various subclasses and the specific methods are described in Table 1 in Appendix C. In addition, for s-stage MIRK methods, it is possible to construct methods of order $p = s + 1$ [22]. This is in general higher order than what is possible to obtain with s-stage explicit Runge–Kutta methods. Further computational gains could also be made by reusing evaluations of the vector field between multiple steps, which using MIRK methods allow for, as explained in Appendix I. The dependency structure on the data S_N of explicit RK (ERK) methods, MIRK methods and the SRNN method [10] is illustrated in Figure 2.

Maximal order of symplectic MIRK methods: From the preceding discussion, it is clear that symplectic MIRK methods are of interest when learning Hamiltonian systems from data, since they combine computational efficiency with the ability to preserve useful, geometric properties. Indeed, symplectic integrators in the training of HNNs have been considered in [9, 10, 11, 12, 13]. The subclass of symplectic MIRK methods is represented by the middle, dark blue field in the Venn diagram of Figure 1. The next result gives an order barrier for symplectic MIRK methods that was, to the best of our knowledge, not known up to this point.

Theorem 4.4. *The maximum order of a symplectic MIRK method is $p = 2$.*

Proof. This is a shortened version of the full proof, which can be found in Appendix F. A MIRK method is a Runge–Kutta method with coefficients $a_{ij} = d_{ij} + v_i b_j$. Requiring d_{ij}, b_i and v_i to satisfy the symplecticity conditions of (5) in addition to D being strictly lower triangular, yields the following restrictions

$$\begin{aligned} b_i d_{ij} + b_i b_j (v_j + v_i - 1) = 0, &\quad \text{if } i \neq j, \\ b_i = 0 \text{ or } v_i = \frac{1}{2}, &\quad \text{if } i = j, \\ d_{ij} = 0, &\quad \text{if } i > j. \end{aligned} \tag{8}$$

These restrictions result in an RK method that could be reduced to choosing a coefficient vector $b \in \mathbb{R}^s$ and choosing stages on the form $k_i = f\big(y_n + \frac{h}{2}\sum_j^s b_j k_j\big)$ for $i = 1, \ldots, s$. It is then trivial to check that this method can only be of up to order $p = 2$. Note that for $s = 1$ and $b_1 = 1$ we get the midpoint method. □

Numerical integrators outside the RK class: While this paper is mainly concerned with MIRK methods, several other types of numerical integrators could be of interest for inverse problems. *Partitioned Runge–Kutta methods* are an extension and not a subclass of RK methods, and can be symplectic and symmetric, while also being explicit for separable Hamiltonian systems. The Störmer–Verlet integrator of order $p = 2$ is one example. Higher order methods of this type are derived in [28] and used for learning Hamiltonian systems in [29, 30]. *Discrete gradient methods* [31, 32] are inverse explicit and well suited to train Hamiltonian neural networks using a modified automatic differentiation algorithm [15]. This method could be extended to higher order methods as shown in [16]. In contrast to symplectic methods, discrete gradient methods preserve the Hamiltonian exactly up to machine precision. A third option is *elementary differential Runge–Kutta methods* [33], where for instance [34] show how to use backward error analysis to construct higher order methods from modifications to the midpoint method. This topic is discussed further in Appendix H, where we also present a novel, symmetric discrete gradient method of order $p = 4$.

5 Mean inverse integrator for handling noisy data

Noisy ODE sample: It is often the case that the samples S_N are not exact measurements of the system, but perturbed by noise. In this paper, we model the noise as independent, normally distributed

perturbations

$$\tilde{y}_n = y(t_n) + \delta_n, \quad \delta_n \sim \mathcal{N}(0, \sigma^2 I), \tag{9}$$

where $\mathcal{N}(0, \sigma^2 I)$ represents the multivariate normal distribution. With this assumption, a standard result from statistics tells us that the variance of a sample-mean estimator with N samples converges to zero at the rate of $\frac{1}{N}$. That is, assuming that we have N samples $\tilde{y}_n^{(1)}, \dots, \tilde{y}_n^{(N)}$, then

$$\text{Var}[\overline{y}_n] = \text{Var}\left[\frac{1}{N}\sum_{j=1}^{N} \tilde{y}_n^{(j)}\right] = \frac{\sigma^2}{N}.$$

Using the inverse injection with the midpoint method, the vector field is evaluated in the average of $\tilde{y}_n$ and $\tilde{y}_{n+1}$, reducing the variance of the perturbation by a factor of two, compared to evaluating the vector field in $\tilde{y}_n$, as is done in all explicit RK methods. Furthermore, considering the whole data trajectory S_N, multiple independent approximations to the same point $y(t_n)$ can enable an even more accurate estimate. This is demonstrated in the analysis presented in Theorem 5.2 and in Figure 4.

Averaging multiple trajectories: In the inverse ODE problem, we assume that there exists an *exact* vector field f whose flow interpolates the discrete trajectories S_N, and the flow of this vector field satisfies the group property (3). The numerical flow $\Phi_{h,f}$ for a method of order p satisfies this property only up to an error $\mathcal{O}(h^{p+1})$ over one step. In the presence of noisy data, compositions of one-step methods can be used to obtain multiple different approximations to the same point $y(t_n)$, by following the numerical flow from different nearby initial values $\tilde{y}_j, j \neq n$, and thus reduce the noise by averaging over these multiple approximations. Accumulation of the local truncation error is expected when relying on points further away from t_n. However, for sufficiently small step sizes h compared to the size of the noise σ, one can expect increased accuracy when averaging over multiple noisy samples.

As an example, assume that we know the points $\{\tilde{y}_0, \tilde{y}_1, \tilde{y}_2, \tilde{y}_3\}$. Then $y(t_2)$ can be approximated by computing the mean of the numerical flows $\Phi_{h,f}$ starting from different initial values:

$$\begin{aligned} \overline{y}_2 &= \frac{1}{3}\big(\Phi_{h,f}(\tilde{y}_1) + \Phi_{h,f} \circ \Phi_{h,f}(\tilde{y}_0) + \Phi^*_{-h,f}(\tilde{y}_3)\big) \\ &\approx \frac{1}{3}\big(\tilde{y}_0 + \tilde{y}_1 + \tilde{y}_3 + h(\Psi_{0,1} + 2\Psi_{1,2} - \Psi_{2,3})\big), \end{aligned} \tag{10}$$

where we by Φ^* mean the adjoint method of Φ, as defined in [8, Ch. V], and we let $\Psi_{n,n+1}$ be the increment of an inverse-explicit numerical integrator, so that

$$\Phi_{h,f}(\tilde{y}_n, \tilde{y}_{n+1}) = \tilde{y}_n + h\Psi_{n,n+1}.$$

For example, for the midpoint method, we have that $\Psi_{n,n+1} = f(\frac{\tilde{y}_n + \tilde{y}_{n+1}}{2})$. When stepping in negative time in (10), we use the adjoint method in order to minimize the number of vector field evaluations, also when non-symmetric methods are used (which implies that we always use e.g. $\Psi_{1,2}$ and not $\Psi_{2,1}$). Note that in order to derive the approximation in (10), repeated use of the inverse injection allows the known points $\tilde{y}_n$ to form an explicit integration procedure, where composition of integration steps are approximated by summation over increments $\Psi_{n,n+1}$. This approximation procedure is presented in greater detail in Appendix D.

Mean inverse integrator: The mean approximation over the whole trajectory $\overline{y}_n$, for $n = 0, \dots, N$, could be computed simultaneously, reusing multiple vector field evaluations in an efficient manner. This leads to what we call the mean inverse integrator. For example, when $N = 3$ we get

$$\begin{bmatrix} \overline{y}_0 \\ \overline{y}_1 \\ \overline{y}_2 \\ \overline{y}_3 \end{bmatrix} = \frac{1}{3}\begin{bmatrix} 0 & 1 & 1 & 1 \\ 1 & 0 & 1 & 1 \\ 1 & 1 & 0 & 1 \\ 1 & 1 & 1 & 0 \end{bmatrix}\begin{bmatrix} \tilde{y}_0 \\ \tilde{y}_1 \\ \tilde{y}_2 \\ \tilde{y}_3 \end{bmatrix} + \frac{h}{3}\begin{bmatrix} -3 & -2 & -1 \\ 1 & -2 & -1 \\ 1 & 2 & -1 \\ 1 & 2 & 3 \end{bmatrix}\begin{bmatrix} \Psi_{0,1} \\ \Psi_{1,2} \\ \Psi_{2,3} \end{bmatrix},$$

and the same structure is illustrated in Figure 3.

Definition 5.1 (Mean inverse integrator)**.** For a sample S_N and an inverse-explicit integrator $\Psi_{n,n+1}$, the mean inverse integrator is given by

$$\overline{Y} = \frac{1}{N}\Big(U\tilde{Y} + hW\Psi\Big) \tag{11}$$

where $\tilde{Y} := [\tilde{y}_0, \dots, \tilde{y}_N]^T \in \mathbb{R}^{(N+1)\times m}$, $\Psi := [\Psi_{0,1}, \dots, \Psi_{N-1,N}]^T \in \mathbb{R}^{N\times m}$.

Finally, $U \in \mathbb{R}^{(N+1)\times(N+1)}$ and $W \in \mathbb{R}^{(N+1)\times N}$ are given by

$$[U]_{ij} := \begin{cases} 0 & \text{if} \quad i = j \\ 1 & \text{else} \end{cases} \qquad \text{and} \qquad [W]_{ij} := \begin{cases} j-1-N & \text{if} \quad j \geq i \\ j & \text{else} \end{cases}.$$

By substituting the known vector field f with a neural network f_θ and denoting the matrix containing vector field evaluations by Ψ_θ such that $\overline{Y}_\theta := \frac{1}{N}(U\tilde{Y} + hW\Psi_\theta)$, we can formulate an analogue to the inverse problem (6) by

$$\arg\min_\theta \left\| \tilde{Y} - \overline{Y}_\theta \right\|. \tag{12}$$

Analysis of sensitivity to noise: Consider the optimization problems using integrators either as one-step methods or MII by (6) resp. (12). We want to investigate how uncertainty in the data $\tilde{y}_n$ introduces uncertainty in the optimization problem. Assume, for the purpose of analysis, that the underlying vector field $f(y)$ is known. Let

$$\mathcal{T}_n^{\text{OS}} := \tilde{y}_n - \Phi_{h,f}(\tilde{y}_{n-1}, \tilde{y}_n),$$
$$\mathcal{T}_n^{\text{MII}} := \tilde{y}_n - [\overline{Y}]_n$$

be the *optimization target* or the expression one aims to minimize using a one-step method (OS) and the MII, where $\overline{Y}$ is given by Definition 5.1. For a matrix A with eigenvalues $\lambda_i(A)$, the spectral radius is given by $\rho(A) := \max_i |\lambda_i(A)|$. An analytic expression that approximates $\rho(\mathcal{T}_n^{\text{OS}})$ and $\rho(\mathcal{T}_n^{\text{MII}})$ by linearization of f for a general MIRK method is provided below.

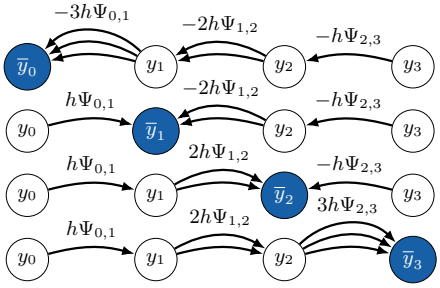

Figure 3: Illustration of the structure of the mean inverse integrator for $N = 3$.

Theorem 5.2. *Let $S_N = \{\tilde{y}_n\}_{n=0}^N$ be a set of noisy samples, equidistant in time with step size h, with Gaussian perturbations as defined by (9) with variance σ^2. Assume that a MIRK integrator $\Phi_{h,f}$ is used as a one-step method. Then the spectral radius is approximated by*

$$\rho_n^{OS} := \rho\left(Var[\mathcal{T}_n^{OS}]\right) \approx \sigma^2 \left\| 2I + hb^T(\mathbb{1} - 2v)\left(f' + f'^T\right) + h^2 Q^{OS} \right\|_2, \tag{13}$$

$$\rho_n^{MII} := \rho\left(Var[\mathcal{T}_n^{MII}]\right) \approx \frac{\sigma^2}{N} \left\| (1+N)I + hP_{nn} + \frac{h}{N}\sum_{\substack{j=0 \\ j\neq n}}^{s} P_{nj} + \frac{h^2}{N} Q^{MII} \right\|_2, \tag{14}$$

where $f' := f'(y_n)$ and P_{nj}, Q^{OS} and Q^{MII} (defined in (24) in Appendix G) are matrices independent of the step size h.

The proof is found in Appendix G. Let $\alpha := b^T(\mathbb{1} - 2v)$ denote the coefficients of the first order term in h of Equation (13). For any explicit RK method we have that $v = 0$ and since $b^T\mathbb{1} = 1$ (method of at least order one) we find that $\alpha_{\text{ERK}} = 1$. Considering the Butcher tableau of MIRK4 in Figure 9 we find that $\alpha_{\text{MIRK4}} = 0$. Thus, as $h \to 0$ we would expect quadratic convergence of MIRK4 and linear convergence of RK4 for ρ_n^{OS} to $2\sigma^2$. Considering MII (14) one would expect linear convergence for ρ_n^{MII} to σ^2 if N is large, as $h \to 0$.

A numerical approximation of ρ_n^{OS} and ρ_n^{MII} could be realized by a Monte-Carlo estimate. We compute the spectral radius $\hat{\rho}_n$ of the empirical covariance matrix of $\mathcal{T}_n^{\text{OS}}$ and $\mathcal{T}_n^{\text{MII}}$ by sampling $5{\cdot}10^3$ normally distributed perturbations δ_n with $\sigma^2 = 2.5 \cdot 10^{-3}$ to each point y_n in a trajectory of $N+1$ points and step size h. We then compute the

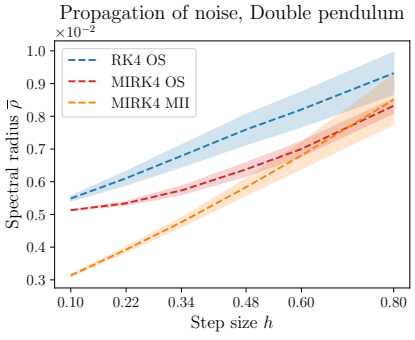

Figure 4: Average of $\overline{\rho}$ over 10 trajectories. Shaded area represent one standard deviation.

trajectory average $\overline{\rho} = \frac{1}{N+1}\sum_{n=0}^{N}\hat{\rho}_n$, fix the end time $T = 2.4$, repeat the approximations for decreasing step sizes h and increasing N and compute the average of $\overline{\rho}$ for 10 randomly sampled trajectories S_N from the double pendulum system. The plot in Figure 4 corresponds well with what one would expect from Theorem 5.2 and confirms that first MIRK (with $v \neq 0$) and secondly MII reduces the sensitivity to noise in the optimization target.

6 Experiments

Methods and test problems: We train HNNs using different integrators and methods in the inverse problem (6). We use MIRK4 together with the MII method and compare to the implicit midpoint method, RK4 and MIRK4 applied as one-step methods, as well as ISO followed by Störmer–Verlet and RK4 integrated over multiple time-steps. The latter strategy, illustrated in Figure 2, was suggested in [10], where Störmer–Verlet is used. Separable networks $H_\theta(q,p) = H_{1,\theta}(q) + H_{2,\theta}(p)$ are trained on data from the Fermi–Pasta–Ulam–Tsingou (FPUT) problem and the Hénon–Heiles system. For the double pendulum, which is non-separable, a fully connected network is used for all methods except Störmer–Verlet, which requires separability in order to be explicit. The Hamiltonians are described in Appendix A and all systems have solutions $y(t) \in \mathbb{R}^4$.

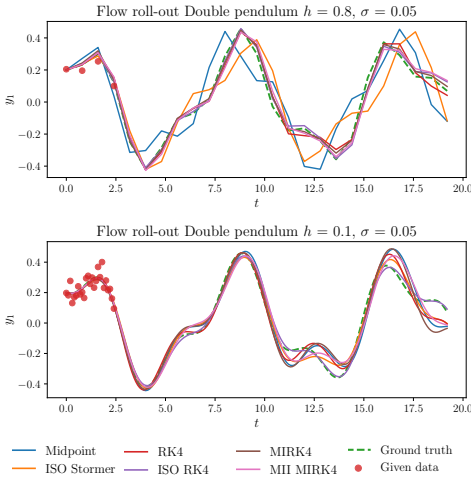

Figure 5: Roll-out in time obtained by integrating over the learned vector fields when training on data from the double pendulum Hamiltonian.

After using the specified integrators in training, approximated solutions are computed for each learned vector field f_θ using the Scikit-learn implementation of DOP853 [35], which is also used to generate the training data. The error is averaged over $M = 10$ points and we find what we call the flow error by

$$e(f_\theta) = \frac{1}{M}\sum_{n=1}^{M} \|\hat{y}_n - y(t_n)\|_2, \quad y(t_n) \in S_M^{\text{test}}, \qquad \hat{y}_{n+1} = \Phi_{h,f_\theta}(y_n). \tag{15}$$

Training data: Training data is generated by sampling $N_2 = 300$ random initial values y_0 requiring that $0.3 \leq \|y_0\|_2 \leq 0.6$. The data $S_{N_1,N_2} = \{\tilde{y}_n^{(j)}\}_{n=0,j=0}^{N_1,N_2}$ is found by integrating the initial values with DOP853 with a tolerance of 10^{-15} for the following step sizes and number of steps: $(h, N_1) = (0.4, 4), (0.2, 8), (0.1, 16)$. The points in the flow are perturbed by noise where $\sigma \in \{0, 0.05\}$. Error is measured in $M = 10$ random points in the flow, within the same domain as the initial values. Furthermore, experiments are repeated with a new random seed for the generation of data and initialization of neural network parameters five times in order to compute the standard deviation of the flow error. The flow error is shown in Figure 6. Additional results are presented in Appendix B.

Neural network architecture and optimization: For all test problems, the neural networks have 3 layers with a width of 200 neurons and $\tanh(\cdot)$ as the activation function. The algorithms are implemented using PyTorch [36] and the code for performing ISO is a modification of the implementation by [10][1]. Training is done using the quasi-Newton L-BFGS algorithm [37] for 20 epochs without batching. This optimization algorithm is often used to train physics-informed neural networks [1] and in this setting it proved to yield superior results in comparison to the often used Adam optimizer. Further details are provided in Appendix E.

Results: As observed in Figure 6 and supported by the analytical result illustrated in Figure 4, the MII approach facilitates more accurate training from from noisy data than one-step methods. However, training with multiple integration steps in combination with ISO yields lower error when RK4 is used

[1] https://github.com/zhengdao-chen/SRNN (CC-BY-NC 4.0 License)

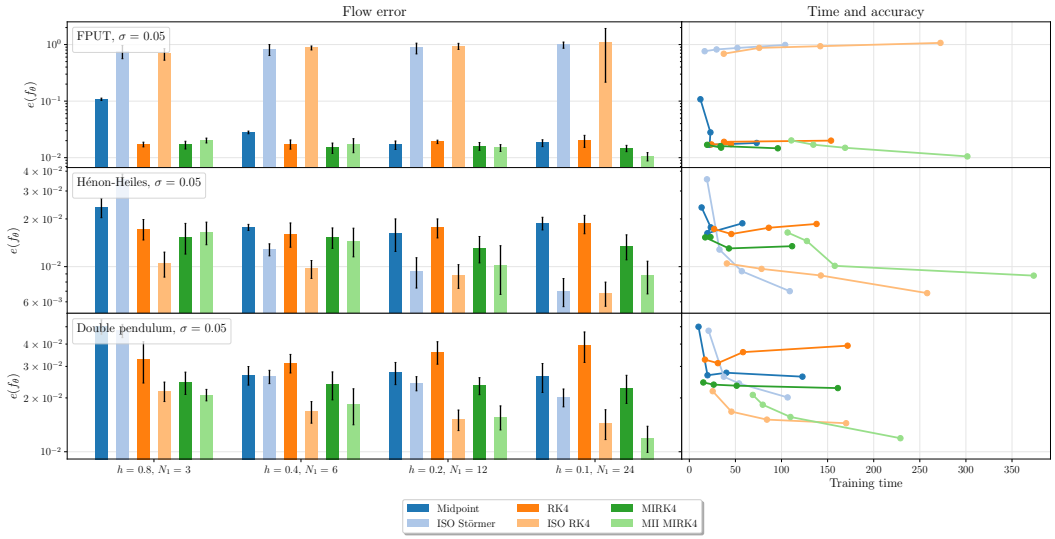

Figure 6: The flow error when learning vector fields using one-step methods directly (Midpoint, RK4 and MIRK4), ISO and multiple time-steps (ISO Störmer and ISO RK4) and MII (MII MIRK4). The error bars display the standard deviation after rerunning 5 experiments on data with $\sigma = 0.05$. The right subplot shows the computational time used in training against the flow error.

for the Hénon–Heiles problem and similar performance as MII on the double pendulum. We notice that the SRNN approach, i.e. ISO with Störmer–Verlet, is improved when switching to RK4, which means sacrificing symplecticity to achieve higher order. The results for FPUT stand out in Figure 6, since both ISO methods have large errors here. The roll-out in time of the learned vector fields is presented in Figure 8 in Appendix B, where the same can be observed. As also could be seen here, the FPUT Hamiltonian gives rise to highly oscillatory trajectories, and the errors observed in Figure 6 might indicate that ISO is ill-suited for this kind of dynamical systems.

Two observations could be made regarding the one-step methods without averaging or ISO. First, it is likely that the midpoint method has weaker performance for large step sizes due to its lower order, compared to both RK4 and MIRK4, despite the fact that it is a symplectic method. The same is clear from Figure 7 in Appendix B, which display the flow error when training on data without noise. Secondly, building on the sensitivity analysis, we observe that MIRK4 consistently attains higher accuracy than RK4, as expected from the Monte-Carlo simulation found in Figure 4.

7 Conclusion

In this work we present the mean inverse integrator, which allows both chaotic and oscillatory dynamical systems to be learned with high accuracy from noisy data. Within this method, integrators of the MIRK class are a key component. To analyse how noise is propagated when training with MII and MIRK, compared to much used explicit methods such as RK4, we developed a sensitivity analysis that is verified both by a Monte-Carlo approximation and reflected in the error of the learned vector fields. Finally, we build on the SRNN [10] by replacing Störmer–Verlet with RK4, and observer increased performance. When also considering the weak performance of the implicit midpoint method, this tells us that order might be of greater importance than preserving the symplectic structure when training HNNs. Both the MIRK methods, the mean inverse integrator and initial state optimization form building blocks that could be combined to form novel approaches for solving inverse problems and learning from noisy data.

Limitations: The experiments presented here assume that both the generalized coordinates q_n and the generalized momenta p_n could be observed. In a setting where HNNs are to model real and not simulated data, the observations might lack generalized momenta [38] or follow Cartesian coordinates, requiring the enforcement of constraints [17, 39]. Combining approaches that are suitable for data that is both noisy and follow less trivial coordinate systems is a subject for future research.

References

[1] Maziar Raissi, Paris Perdikaris, and George E Karniadakis. Physics-informed neural networks: A deep learning framework for solving forward and inverse problems involving nonlinear partial differential equations. *Journal of Computational physics*, 378:686–707, 2019.

[2] Christopher Rackauckas, Yingbo Ma, Julius Martensen, Collin Warner, Kirill Zubov, Rohit Supekar, Dominic Skinner, Ali Ramadhan, and Alan Edelman. Universal differential equations for scientific machine learning. Aug 2020.

[3] Ricky TQ Chen, Yulia Rubanova, Jesse Bettencourt, and David K Duvenaud. Neural ordinary differential equations. *Advances in neural information processing systems*, 31, 2018.

[4] Zongyi Li, Nikola Kovachki, Kamyar Azizzadenesheli, Burigede Liu, Kaushik Bhattacharya, Andrew Stuart, and Anima Anandkumar. Fourier neural operator for parametric partial differential equations. *arXiv preprint arXiv:2010.08895*, 2020.

[5] Sam Greydanus, Misko Dzamba, and Jason Yosinski. Hamiltonian neural networks. *CoRR*, abs/1906.01563, 2019.

[6] Herbert Goldstein, Charles Poole, and John Safko. *Classical Mechanics*. Addison Wesley, 3 edition, 2001.

[7] Benedict Leimkuhler and Sebastian Reich. *Simulating Hamiltonian Dynamics*. Cambridge Monographs on Applied and Computational Mathematics. Cambridge University Press, 2005.

[8] Ernst Hairer, Christian Lubich, and Gerhard Wanner. *Geometric Numerical Integration: Structure-Preserving Algorithms for Ordinary Differential Equations; 2nd ed.* Springer, Dordrecht, 2006.

[9] Christian Offen and Sina Ober-Blöbaum. Symplectic integration of learned Hamiltonian systems. *Chaos: An Interdisciplinary Journal of Nonlinear Science*, 32(1):013122, 2022.

[10] Zhengdao Chen, Jianyu Zhang, Martin Arjovsky, and Léon Bottou. Symplectic recurrent neural networks. In *International Conference on Learning Representations*, 2020.

[11] Aiqing Zhu, Pengzhan Jin, and Yifa Tang. Deep Hamiltonian networks based on symplectic integrators. *arXiv preprint arXiv:2004.13830*, 2020.

[12] Marco David and Florian Méhats. Symplectic learning for Hamiltonian neural networks. *arXiv preprint arXiv:2106.11753*, 2021.

[13] Pengzhan Jin, Zhen Zhang, Aiqing Zhu, Yifa Tang, and George Em Karniadakis. SympNets: Intrinsic structure-preserving symplectic networks for identifying Hamiltonian systems. *Neural Networks*, 132:166–179, 2020.

[14] Aiqing Zhu, Pengzhan Jin, Beibei Zhu, and Yifa Tang. Inverse modified differential equations for discovery of dynamics. *arXiv preprint arXiv:2009.01058*, 2020.

[15] Takashi Matsubara, Ai Ishikawa, and Takaharu Yaguchi. Deep energy-based modeling of discrete-time physics. *Advances in Neural Information Processing Systems*, 33:13100–13111, 2020.

[16] Sølve Eidnes. Order theory for discrete gradient methods. *BIT*, 62(4):1207–1255, 2022.

[17] Elena Celledoni, Andrea Leone, Davide Murari, and Brynjulf Owren. Learning Hamiltonians of constrained mechanical systems. *J. Comput. Appl. Math.*, 417:Paper No. 114608, 12, 2023.

[18] Alvaro Sanchez-Gonzalez, Victor Bapst, Kyle Cranmer, and Peter Battaglia. Hamiltonian Graph Networks with ODE Integrators.

[19] Gerhard Wanner and Ernst Hairer. *Solving ordinary differential equations II*, volume 375. Springer Berlin Heidelberg, 1996.

[20] Senwei Liang, Zhongzhan Huang, and Hong Zhang. Stiffness-aware neural network for learning Hamiltonian systems. 2022.

[21] Jeff R Cash. A class of implicit Runge–Kutta methods for the numerical integration of stiff ordinary differential equations. *Journal of the ACM (JACM)*, 22(4):504–511, 1975.

[22] K Burrage, FH Chipman, and Paul H Muir. Order results for mono-implicit Runge–Kutta methods. *SIAM journal on numerical analysis*, 31(3):876–891, 1994.

[23] Håkon Noren. Learning Hamiltonian systems with mono-implicit Runge–Kutta methods. *arXiv preprint, arXiv:2303.03769*, 2023.

[24] Harsh Sharma, Nicholas Galioto, Alex A Gorodetsky, and Boris Kramer. Bayesian identification of nonseparable Hamiltonian systems using stochastic dynamic models. In *2022 IEEE 61st Conference on Decision and Control (CDC)*, pages 6742–6749. IEEE, 2022.

[25] W. M. G. van Bokhoven. Efficient higher order implicit one-step methods for integration of stiff differential equations. *BIT*, 20(1):34–43, 1980.

[26] J. R. Cash and A. Singhal. Mono-implicit Runge–Kutta formulae for the numerical integration of stiff differential systems. *IMA J. Numer. Anal.*, 2(2):211–227, 1982.

[27] Sølve Eidnes, Alexander J Stasik, Camilla Sterud, Eivind Bøhn, and Signe Riemer-Sørensen. Pseudo-Hamiltonian neural networks with state-dependent external forces. *arXiv preprint, arXiv:2206.02660*, 2022.

[28] Haruo Yoshida. Construction of higher order symplectic integrators. *Physics letters A*, 150(5-7):262–268, 1990.

[29] Shaan A Desai, Marios Mattheakis, and Stephen J Roberts. Variational integrator graph networks for learning energy-conserving dynamical systems. *Physical Review E*, 104(3):035310, 2021.

[30] Daniel DiPietro, Shiying Xiong, and Bo Zhu. Sparse symplectically integrated neural networks. *Advances in Neural Information Processing Systems*, 33:6074–6085, 2020.

[31] GRW Quispel and Grant S Turner. Discrete gradient methods for solving ODEs numerically while preserving a first integral. *Journal of Physics A: Mathematical and General*, 29(13):L341, 1996.

[32] Robert I McLachlan, G Reinout W Quispel, and Nicolas Robidoux. Geometric integration using discrete gradients. *Philosophical Transactions of the Royal Society of London. Series A: Mathematical, Physical and Engineering Sciences*, 357(1754):1021–1045, 1999.

[33] Ander Murua. *Métodos simplécticos desarrollables en P-series*. PhD thesis, PhD thesis. Valladolid: Universidad de Valladolid, 1995.

[34] Philippe Chartier, Ernst Hairer, and Gilles Vilmart. Numerical integrators based on modified differential equations. *Mathematics of Computation*, 76(260):1941–1953, October 2007.

[35] J.R. Dormand and P.J. Prince. A family of embedded Runge–Kutta formulae. *Journal of Computational and Applied Mathematics*, 6(1):19–26, 1980.

[36] Adam Paszke, Sam Gross, Francisco Massa, Adam Lerer, James Bradbury, Gregory Chanan, Trevor Killeen, Zeming Lin, Natalia Gimelshein, Luca Antiga, et al. PyTorch: An imperative style, high-performance deep learning library. *Advances in neural information processing systems*, 32:8026–8037, 2019.

[37] Jorge Nocedal and Stephen J Wright. *Numerical optimization*. Springer, 1999.

[38] Yuhan Chen, Takashi Matsubara, and Takaharu Yaguchi. Neural symplectic form: learning hamiltonian equations on general coordinate systems. *Advances in Neural Information Processing Systems*, 34:16659–16670, 2021.

[39] Marc Finzi, Ke Alexander Wang, and Andrew Gordon Wilson. Simplifying Hamiltonian and Lagrangian neural networks via explicit constraints. *arXiv preprint arXiv:2010.13581*, 2020.

[40] Enrico Fermi, P Pasta, Stanislaw Ulam, and Mary Tsingou. Studies of the nonlinear problems. Technical report, Los Alamos National Lab.(LANL), Los Alamos, NM (United States), 1955.

[41] E. Hairer, S. P. Nørsett, and G. Wanner. *Solving ordinary differential equations. I*, volume 8 of *Springer Series in Computational Mathematics*. Springer-Verlag, Berlin, second edition, 1993. Nonstiff problems.

[42] P. H. Muir. Optimal discrete and continuous mono-implicit Runge-Kutta schemes for BVODEs. *Adv. Comput. Math.*, 10(2):135–167, 1999.

[43] J. R. Cash and D. R. Moore. A high order method for the numerical solution of two-point boundary value problems. *BIT*, 20(1):44–52, 1980.

[44] Philippe Chartier. Symmetric Methods. In Björn Engquist, editor, *Encyclopedia of Applied and Computational Mathematics*, pages 1439–1448. Springer, Berlin, Heidelberg, 2015.

[45] J. R. Cash and A. Singhal. High order methods for the numerical solution of two-point boundary value problems. *BIT*, 22(2):184–199, 1982.

[46] Pauli Virtanen, Ralf Gommers, Travis E. Oliphant, Matt Haberland, Tyler Reddy, David Cournapeau, Evgeni Burovski, Pearu Peterson, Warren Weckesser, Jonathan Bright, Stéfan J. van der Walt, Matthew Brett, Joshua Wilson, K. Jarrod Millman, Nikolay Mayorov, Andrew R. J. Nelson, Eric Jones, Robert Kern, Eric Larson, C J Carey, İlhan Polat, Yu Feng, Eric W. Moore, Jake VanderPlas, Denis Laxalde, Josef Perktold, Robert Cimrman, Ian Henriksen, E. A. Quintero, Charles R. Harris, Anne M. Archibald, Antônio H. Ribeiro, Fabian Pedregosa, Paul van Mulbregt, and SciPy 1.0 Contributors. SciPy 1.0: Fundamental Algorithms for Scientific Computing in Python. *Nature Methods*, 17:261–272, 2020.

[47] Philippe Chartier, Ernst Hairer, and Gilles Vilmart. Numerical integrators based on modified differential equations. *Math. Comp.*, 76(260):1941–1953, 2007.

[48] Ge Zhong and Jerrold E. Marsden. Lie-Poisson Hamilton-Jacobi theory and Lie-Poisson integrators. *Phys. Lett. A*, 133(3):134–139, 1988.

[49] Takashi Matsubara and Takaharu Yaguchi. FINDE: Neural differential equations for finding and preserving invariant quantities. *arXiv preprint, arXiv:2210.00272*, 2022.